Spectral Characterization of Spacecraft Materials used in Hypervelocity Impact Testing

Jacqueline A. Reyes[a], Heather M. Cowardin[b], Karin Fulford[c], Ryan C. Hoffmann[d], Vanessa Murray[e], Dale C. Ferguson[d], Elena Plis[f,g], Daniel P. Engelhart[g]

[a]University of Texas at El Paso, 500 W. University Ave., El Paso, TX, 79968, USA;
[b]NASA Johnson Space Center, Orbital Debris Program Office, Houston, TX, 77058, USA;
[c]University of New Mexico/COSMIAC, 2350 Alamo Ave. SE, Suite 300, Albuquerque, New Mexico 87106, USA;
[d]Air Force Research Laboratory, Space Vehicles Directorate, Kirtland AFB, Albuquerque, NM, 87117, USA;
[e]National Research Council at Air Force Research Laboratory, Albuquerque, NM 87117 USA;
[f]Georgia Tech Research Institute, 925 Dalney St NW, Atlanta, GA 30318;
[g]Assurance Technology Corporation, 84 South Street, Carlisle, MA, 01741, USA

ABSTRACT

The increasing number of successfully deployed space missions have resulted in an increased density of man-made objects positioned in orbital domains near Earth. With this steady accumulation of objects in space, it is becoming more imperative to characterize spacecraft materials, which may ultimately be contributors to the orbital debris population. In order to ascertain the potential damage from orbital debris, a laboratory hypervelocity impact test was conducted using a 56-kg modern spacecraft representative satellite (DebriSat) to simulate a catastrophic fragmentation event in low Earth orbit. In an effort to identify unique, material-specific spectroscopic markers, a select number of the spacecraft materials used to construct DebriSat were analyzed using reflectance spectroscopy as a characterization technique for assessment on material type according to optical features. Spectral measurements of DebriSat materials analyzed prior to the laboratory impact are presented in this paper. These data provide a spectral characterization baseline for modern-day spacecraft materials in their pristine conditions and are compared to each other to distinguish spectra of materials belonging to different classifications with an effort of grouping them using color index. The ongoing efforts to classify materials utilizing their reflectance spectroscopic fingerprint are discussed in this study.

Keywords: spectral reflectance measurements; hypervelocity impact test; spacecraft materials; optical characterization; color index.

1. INTRODUCTION

As the demand for space exploration continues to thrive, it can be expected that increasing amounts of space hardware articles will populate the orbital regimes near Earth. With higher quantities of objects residing in low Earth orbit (LEO) and geosynchronous Earth orbit (GEO), objects will face increased risk of undergoing collisions with other nearby objects or risk of being impacted by micrometeoroids. These destructive events can result in the production of orbital debris. Debris objects can be considered to fall into as small a size within submillimeter range [1] or can be as large as a full satellite that has lost communication and is no longer functional. Approximately half of the many collision events that occur in LEO can occur from speeds of more than 14 km/s [2]. Debris size, speed, and material are factors that contribute to the magnitude of damage caused by such objects. The persistently increasing orbital debris population has amounted to 15,214 spent rocket body and debris that have been cataloged by the U.S. Space Surveillance Network as of 04 October 2020 [3]. It is vital that orbital debris undergo investigations to track debris position, speed, and material to assess any potential hazards that are associated with it.

In order to help observe the resulted behavior from a spacecraft that experiences a major destructive event in LEO, a laboratory hypervelocity impact test was executed on a 56-kg high-fidelity space satellite known as DebriSat [4]. This simulated catastrophic satellite event was developed and executed with the objective of performing a thorough characterization analysis on all fragmentations, down to 2 mm in size, generated as a result of impact. This data would then be used to help better understand the orbital debris environment that is increasingly populated of fragmented space materials, therefore enhancing space situational awareness. One of the analysis efforts underway is to optically characterize spacecraft materials to 1) convert optical brightness to size and 2) classify materials with their respective densities and shapes to inform damage equations associated with typical modern-day spacecraft materials. Classifying debris can also deliver a degree of knowledge about the fragmentation event if that debris object can be linked back to its parent object. Specific optical characterization of resident space objects has been known to help assess material composition of the targets leading to more refined knowledge on the status/health of the target. For example, comparing the material composition of a target pre-launch and during in- orbit may provide insight into whether a shedding event or potentially other fragmentation event occurred that could lead to orbital debris generation.

Debris and objects in space can be characterized through analysis of their reflectance response from illumination impinging on its surface. This is due to specific features present in a reflectance signature for any given material, serving as a fingerprint that can be used to identify the visual and chemical make-up of the target item. Reflectance spectroscopy is employed as a tool to measure the reflectivity response of a sample material for this reason. In the 1970's asteroid examinations were performed using astronomical reflectance spectroscopy (ARS) and this technique expanded in the 1990's to serve as a tool for characterizing spacecraft materials in orbit [5]. Reflectance measurements performed in a laboratory setting can be a useful reference for spectroscopic or photometric data obtained remotely.

The aim for this study is to analyze the reflectance signatures of various spacecraft materials, including DebriSat materials, and calculate their color indices using Sloan Digital Sky Survey (SDSS) filter passbands with the intention of identifying optical trends between materials belonging to different classifications. Though reflectance spectroscopy has been employed by various entities to characterize materials [6, 7, 8, 9, 10], there is room for advancement in enhancing the data within spectral libraries to group/sort materials having similar optical features into families by color index for the feasibility in assessing materials based on their general physical properties such as density. While ECOSTRESS [11] and USGS [12] spectral libraries effectively house spectral data for a variety of man-made materials, they currently only provide a single spectral plot per material and are heavily geared toward minerals, vegetation, and other natural materials.

Furthermore, reflectance spectra are usually presented and analyzed as one plot per material but are not grouped by density or other intrinsic, physical material properties from spectral features for easier assessment of distinguishing materials by classification. It has been attempted by [13] for UV-VIS using principal component analysis (PCA) for textile fibers, and by [14] for urban materials with a focus on mineral classification, and by [15] using Johnson/Bessel filters with a focus on area-to-mass (A/m) ratio, amongst others who have aimed to improve spectral libraries in various aspects [16, 17], but can be furthered for specific space materials throughout the visible (VIS), near infrared (NIR), and shortwave infrared (SWIR) regions using SDSS color indices from reflectance spectra as a means for classification.

With the large variations in human-made materials (not just composition, but also in coated/painted surfaces), it becomes increasingly difficult to correlate optical measurements of targets from ground-based assets to that of nearly 1,000 laboratory acquired measurements [18] available. Secondly, machine learning is being utilized more for autonomous pattern matching to associate data [19]. Therefore, the goal is to use a taxonomy approximation of the laboratory acquired spectral data to group similar material responses provided the uncertainty with unmixing models to identify specific materials from integrated material

compositions. If materials can be sorted by metals, polymers, composites, etc. from their reflectance spectra, this can in turn improve spectral libraries that serve to catalogue a wide variety of constituents. Furthermore, knowledge of the taxonomy-based relationships that a debris material observed remotely falls into can provide information related to that object's density, an advantageous approach to determine hazards associated with that material when traveling at elevated speed in orbit.

2. MATERIALS & METHODS

2.1. DebriSat Experimentation

The DebriSat project initiated with collaborations between National Aeronautics and Space Administration (NASA) Orbital Debris Program Office (ODPO), the Air Force Space and Missile Systems Center (SMC), The Aerospace Corporation (Aerospace), the University of Florida (UF), and the Air Force Arnold Engineering Development Complex (AEDC) [4]. This project aimed to mimic a destructive breakup event of a spacecraft residing in LEO. To accomplish this a 56-kg class spacecraft, "DebriSat", was designed and constructed in comparable fashion to modern satellites positioned in LEO. [4]. This developed "DebriSat" spacecraft was then placed inside a chamber with walls formed of soft catch panels where a hypervelocity impact test was executed onto the DebriSat target. The impact test employed a projectile (8.6 cm x 9 cm, 570 g) fabricated as a nylon cap with a hollow aluminum cylinder embedded in it [4]. The impact of the projectile onto the DebriSat spacecraft was delivered using a two-stage light gas gun, ultimately administering an impact speed of 6.8 km/s and generating approximately 85,000 material fragments that were collected on the soft catch panel walls of the chamber [4]. More details regarding the DebriSat experiment can be found in [4].

2.2. Materials

DebriSat was constructed with materials that are frequently used in space hardware design to resemble what a conventional spacecraft prepared for life in orbit would be composed of. Its design was derived from modern satellites observed in LEO [20, 21]. Some materials to note used in the construction of DebriSat included Ultra Triple Junction (UTJ) solar cells, 6061 aluminum alloy components coated with various colored paints, a copper colored Kapton® polyimide film (used in the Multi-layered Insulation blanket), carbon fiber composites, and different colored printed circuit boards.

Solar cells used in space hardware are fabricated as single- or multi- junction semiconductors containing InGaP, GaAs, Ge or Si sub-cells [22, 23]. The UTJ solar cells used in assembling DebriSat had a GaInP2/GaAs/Ge structure above a germanium substrate and were topped with an anti-reflective cover glass [4]. Photovoltaics are vital constituents in space design, for they provide necessary power to a functional spacecraft and are therefore repeatedly used in the space industry. For this reason, it can be deduced that an abundant amount of solar cells are inhabiting LEO and GEO and their optical signatures should be understood thoroughly to support remote observations.

Space applications often use 6061 aluminum alloy as a preferred material for constructing space hardware due to its high strength-to-weight ratio, thermal conductivity, corrosion resistance, low cost, and its ability to be easily anodized [24, 25]. They have an acceptable density for use in space applications compared to other metals, resulting in 2.70 g/cm^3 [26, 27, 28]. DebriSat was composed of many 6061 aluminum alloys that were coated with either red, magenta, gold, blue, or black paint, or were unpainted but had an anodized coating. Anodizing aluminum introduces an oxide coating on the surface of the alloy that will provide enhanced corrosion and abrasion resistance [25]. This makes them suitable for use in space applications as protective materials to withstand impacts and desirable for their ability to inhibit surface degradation caused by space plasma [24, 29, 30]. 6061 aluminum alloys have proven to be an effective material in the space

industry for its capacity to sustain life in orbit and will likely continue to be frequently implemented in future spacecraft missions. It was numerously incorporated on DebriSat for these reasons.

Multi-layered insulation (MLI) is regularly implemented to cover the exterior surfaces of numerous spacecraft deployed in orbit. It is an essential component that serves to protect solid rocket motors, propellant tanks, and like components from reaching raised temperatures due to the harsh space environment while simultaneously hindering those articles from experiencing their own loss of heat [31]. It is postulated that high-area-to-mass-ratio (HAMR) objects largely consist of the individual layers that form MLI. Kapton® is a polyimide film that is a vital layer of MLI since it is durable, chemically inert, and can withstand elevated temperature and radiation conditions [32]. It has a density of 1.42 g/cm^3 [33]. Kapton® was therefore included in the DebriSat material design and analyzed in this study. A Kapton® polyimide film, manufactured by E.I. du Pont de Nemours and Co., was used in the DebriSat MLI. Trade names and trademarks are used in this report for identification only. Their usage does not constitute an official endorsement, either expressed or implied, by the National Aeronautics and Space Administration.

Carbon fiber composites are making a dramatic impact in modern space design applications. DebriSat included a Composite Overwrapped Pressure Vessel (COPV) and gold shimmer composite within its structure. It is worth noting that the gold shimmer composite was still that of a black carbon fiber composite, but its surface had a gold shimmer visual appearance. These two components were configured with a 6061-T6 aluminum alloy honeycombed core embedded within a Tory T1000 carbon fiber composite. Toray composites have been frequently utilized in space, military, and commercial applications based on their tensile strength (924 ksi) and rather low density (1.8 g/cm^3) [34, 35]. Carbon composites are produced having numerous carbon fibers arranged in a multi-directional orientation to achieve isotropic material properties. Like aluminum alloys, carbon fiber composites have a high strength-to-weight ratio [36], making them excellent candidates for modern spacecraft design.

Printed circuit boards (PCB's) that are space approved materials are often those of FR-4 epoxy composite laminate [37] or PTFE fiberglass [38]. These polymer-based composites can be expected to include quantities of organic content within the material chemistry. FR-4 epoxy has a density of 1.90 g/cm^3 and water absorption of 0.10% [39], whereas PTFE fiberglass laminate circuit board substrate has a density of 2.23 g/cm^3 and water absorption of 0.02% [40]. Four different colored printed circuit boards, each supplied by different manufacturers, were included on DebriSat and analyzed in this study.

2.3. Spectral Measurements

Reflectance spectroscopy is a technique that can be applied toward remote optical measurements for material characterization and optical size calculations from albedo. Spectral measurements were performed on all selected DebriSat materials in this work prior to hypervelocity impact for a pre-characterization of the materials that would be fragmented upon impact. Test configuration involved the material specimen to be placed flat on a horizontal surface representing the origin of set-up, while an illumination source and a spectroradiometer were positioned approximately 45° to that of the specimen and directly opposite to each other. The spectroradiometer employed was an Analytical Spectral Device (ASD) field spectrometer with range capability between 350-2500 nm, and illumination was provided by a quartz lamp. The ASD was calibrated before and during testing using a white reference material (Spectralon) with a high lambertian surface; delivering a near perfect reflective signature. Measurements were performed in the Optical Measurements Center (OMC) at NASA's Johnson Space Center which allowed for an ideal dark lab environment, providing optimal reflectance results specific to each specimen of interest and minimizing any interference of scattered light.

2.4. Color Index

The color index, or ratio of brightness between two filter passbands, for each material analyzed in this work was determined using Sloan Digital Sky Survey (SDSS) filters [41]. Brightness (I) can be calculated from summing the area under a material's reflectance curve between each incremental wavelength. The area ($Area$) under the curve is estimated using the formula:

$$Area_f = \left(\frac{\left(R_f + R_{f+1}\right)}{2}\right) * (\lambda_{f+1} - \lambda_f) \quad (1)$$

taken from calculating the area of a trapezoid where R represents the reflectance value of the measured material at a given wavelength (λ), and subscript f is used to indicate that each of the respective variables correspond to values within the passband of a given SDSS filter. The calculated $Area$ for filter f can then be substituted into the equation:

$$I = \sum_{\lambda_1}^{\lambda_2} Area_f \quad (2)$$

to determine the brightness (I) of a material between $\lambda_1$and λ_2, representing the wavelength at the onset and at the end of the filter's passband range respectively. Having calculated the brightness (I) for one filter, this method can be repeated for a different SDSS filter, and two filters can be compared to each other using:

$$f1' - f2' = -2.5 \log_{10}\left(\frac{I_{f1}}{I_{f2}}\right) \quad (3)$$

where $f_1$and f_2 represent the two different filter bands being used. This will generate a color index value for the material being measured. For this study, g' band (406-544 nm), the r' band (558-682 nm), the i' band (705-835 nm), and the z' band (839-1094 nm) were chosen for analysis to provide various color index outcomes using different filters that could potentially lead toward optical trends between material classifications.

3. RESULTS & DISCUSSION

A total of 14 different material samples had their reflectance signature measured in the visible (VIS), near infrared (NIR), and shortwave infrared (SWIR) regions of the spectrum. The features observed from each of the reflectance signatures in this study can be used to help understand the physical appearance and chemical makeup of the measured materials with the intent of possibly classifying them further into grouped families. Significant features in VIS (350-700 nm), NIR (700-1300 nm), and SWIR (1300-2500 nm) that were present in one or more of the analyzed materials are outlined in Table 1. The 6061 aluminum alloys and the circuit boards of various colors have their own reflectance plots illustrated below to show the similarities and differences between alike materials with only pigment as a variable. Reflectance results involving the DebriSat samples from different material classifications are also shown and superimposed in one plot below for comparison.

The visible region (350-700 nm) of the electromagnetic spectrum is responsible for the ability to detect the pigmentation of an article [6]. This occurs because the illumination that impinges on a sample surface will excite electrons, causing them to occupy higher energy sites and result in different colors of light [42]. The blue painted alloy sample resulted in an initial reflectance at ~400 nm followed by absorption throughout the remainder of the VIS region (Fig. 1). The gold and red painted alloys had relatively low absorption at the onset of the VIS regime beginning at 400 nm but produced evident rise in reflection at 600 and 650 nm

respectively. However, the alloy sample that was painted magenta exhibited a notable increase in reflectance at 400 nm about 2.5 times that of the gold and red painted samples, followed by some level of absorption before reaching ~600 nm where its reflectance curve significantly increased yet again, agreeing with the necessary blue and red color components used to produce magenta. As expected, the black painted alloy was consistently high in absorption throughout the entirety of the visible region until reaching NIR at ~800 nm. The unpainted anodized 6061 aluminum alloy exhibited a rather high reflectance throughout VIS, making it stand apart from all other painted metal samples. This is likely due to the substantial reflectivity often perceived in bare metals [42].

Table 1. Absorption feature details present in the VIS/NIR/SWIR reflectance data for the DebriSat samples.

Wavelength (nm)	Feature	Cause(s)
350-700	High absorption	Black color
350-700	Relatively high absorption	Brown color
400	Sharp increase in reflectance	Blue color
550	Increase in reflectance	Green color
600	Sharp increase in reflectance	Gold color
650	Sharp increase in reflectance	Red color
850	Prominent absorption dip	Aluminum content
1400	Absorption dip	O-H
1700	Asymmetric absorption doublet	O-H, first overtone
1900	Single absorption dip	C-O, O-H, second overtone
1950	Single absorption dip	O-H, second overtone
2180	Asymmetrical absorption doublet	N-H, second overtone C-H, C-O, C=O stretches
2200	Broad absorption feature	C-H
2300	Prominent single absorption dip	C-H, N-H stretches
2450	Low intensity absorption dip	O-H

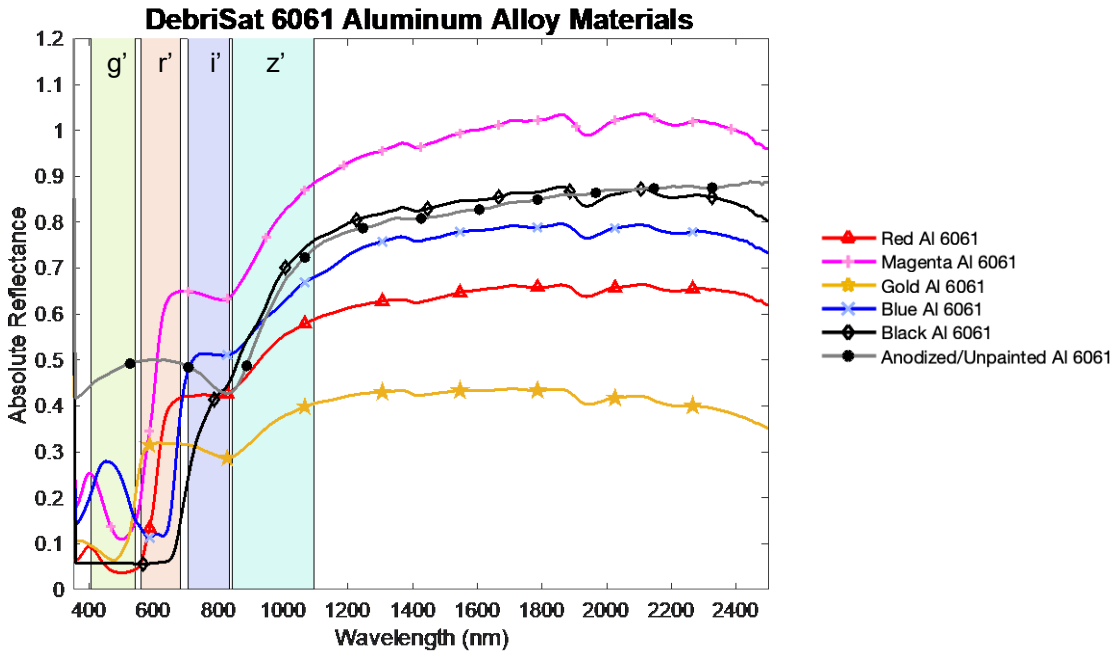

Figure 1. Absolute reflectance of red, magenta, gold, blue, black, and anodized unpainted 6061 aluminum alloy samples in their pre-impact condition. The g', r', i', and z' SDSS filter passbands are depicted in the spectral plot for reference.

Common between all 6061 aluminum alloy sample reflectance signatures (painted or not) is the absorption feature present at 850 nm; a typical indicator of aluminum content within a material that is consistent with literature [4, 12, 43, 44]. In the SWIR regime, all painted alloy samples demonstrated common absorption behavior with a pronounced absorption feature at ~1950 nm, a less pronounced absorption feature at 1400 nm, and broad absorption at 2200 nm (Fig. 1). The small feature present at 1400 nm can be attributed to O-H bend in the first overtone infrared (IR) region associated with water from the chemistry of the sample surface [45]. The absorption dip near 1950 nm is also caused by O-H stretch, but in the second overtone IR region, associated with water and other organics, while the broad feature centered around 2200 nm can be associated with C-H chemical bonds [4, 6, 44, 45, 46]. However, the unpainted anodized metal sample did not exhibit any of the previously described absorption qualities in SWIR, suggesting a lack of organic content that was present in the painted alloy correlatives. Furthermore, the evident difference in reflectance in the g' band between the unpainted and painted alloy samples will lead to a separation in color index values in this passband for the materials. These optical differences between painted and unpainted metals can offer a step towards identifying different classifications of materials remotely with increased confidence.

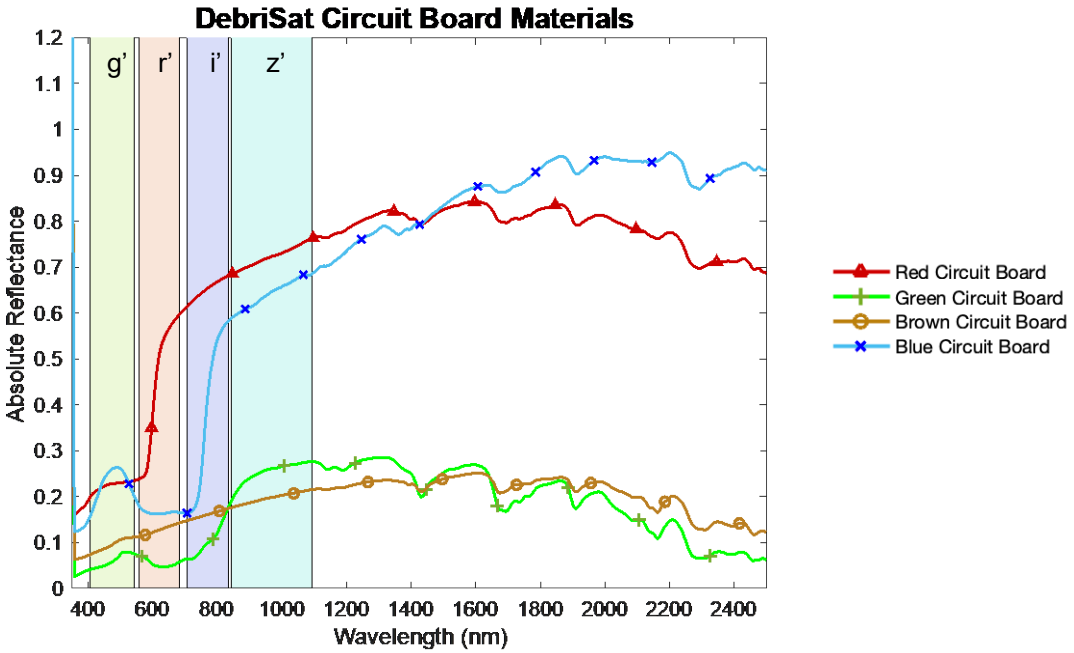

Figure 2. Absolute reflectance spectra of red, green, brown, and blue printed circuit board samples in their pre-impact condition. The g', r', i', and z' SDSS filter passbands are depicted in the spectral plot for reference.

Alike what was described for the painted 6061 aluminum alloys in the VIS region, the DebriSat red, green, brown, and blue circuit board samples exhibit optical properties between 350-700 nm that differentiate each of them by color. The red circuit board demonstrated high absorption throughout the lower wavelengths of VIS until reaching ~650 nm where reflectance peaked, and blue and green circuit boards produced evident quantities of reflectivity at 500 nm and 550 nm respectively, while absorbing all other wavelengths in the visible regime (Fig. 2). Contrarily, the brown PCB was largely absent of any notable features in VIS but still displayed levels of reflectance greater than 0.1 in this region possibly due to the multiple colors required to produce brown. All four circuit board reflectance signatures resulted in near identical absorption features throughout NIR and SWIR, regardless of their manufacturer. The asymmetrical absorption doublets present at ~1400 nm and ~1700 nm for all circuit board samples are likely related to O-H bond vibrations in the first overtone (associated with water) and C-H stretch in the second overtone infrared (IR) region respectively [6, 45]. At 1900 nm, the prominent absorption feature can be attributed to C-O or O-H bonds in the second overtone band [6, 45]. The asymmetrical absorption doublet at 2180 nm, more apparent in the

green and brown circuit board samples, are likely caused by N-H bends in the second overtone IR band, or C-H, C-O, or C=O stretches [6, 45]. Absorption features located at 2300 nm and 2450 nm are associated with C-H and N-H stretches [6, 44], and OH absorption bands [47] respectively.

From the 14 DebriSat material samples measured in this work, a handful of 7 were selected in order to compare the reflectance signature of articles from different material classifications. The UTJ solar cell, unpainted 6061 aluminum alloy, Kapton®, and the gold shimmer and black COPV composites have their absolute reflectance signature plotted for comparison (Fig. 3). Additionally, the red painted 6061 aluminum alloy and the red printed circuit board were included to represent the colored alloys and circuit board categories of DebriSat materials respectively.

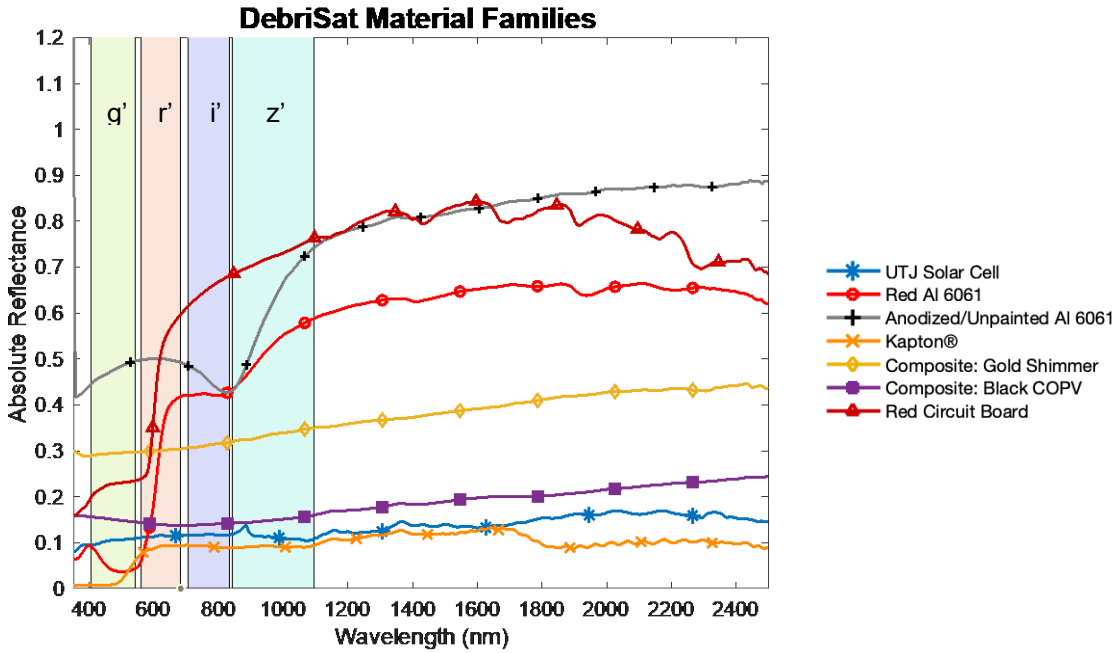

Figure 3. Absolute reflectance spectra of a UTJ solar cell coupon, black painted 6061 aluminum alloy, unpainted anodized 6061 aluminum alloy, MLI Kapton® polyimide sheet, gold shimmer composite, black COPV composite, and a brown circuit board used for DebriSat in their pre-impact conditions. The g', r', i', and z' SDSS filter passbands are depicted in the spectral plot for reference.

The UTJ solar cell produced a consistently low reflectance curve throughout the entirety of the 350-2500 nm range, similar to the MLI Kapton® and black COPV composite samples, however the solar cell differentiates itself from all other materials measured by producing a pronounced peak in reflectance at ~850 nm indicating that the cell is germanium based [4]. The two composite samples exhibited reflectance signatures akin to each other by remaining steadily featureless throughout VIS and NIR, though the gold shimmer composite was 2x times greater in absolute reflectance than its black COPV counterpart, likely due to the gold shine on its surface. The Kapton® sample illustrates its orange color by rising in reflectance near ~550 in VIS, while the red painted alloy and red circuit board don't have increased reflection until reaching ~650 nm as expected.

The 6061 aluminum alloy samples are the only materials that result with an absorption feature at 850 nm in their reflectance curve, singling them out as aluminum related metals. However, the red painted alloy contains absorption features in SWIR that are absent in the unpainted alloy, differentiating painted and unpainted surfaces. The two materials that resulted in the most apparent organic features in their reflectance signatures throughout NIR and SWIR are the circuit board and painted 6061 aluminum alloys. This is likely due to the organic chemical content in paints and in polymer-based PCB'S. Regardless of surface color,

optical features present in a material's reflectance signature in NIR and SWIR beyond 800 nm can be used to aid in differentiating between polymeric, metallic, composite, and semiconductor photovoltaic material classifications.

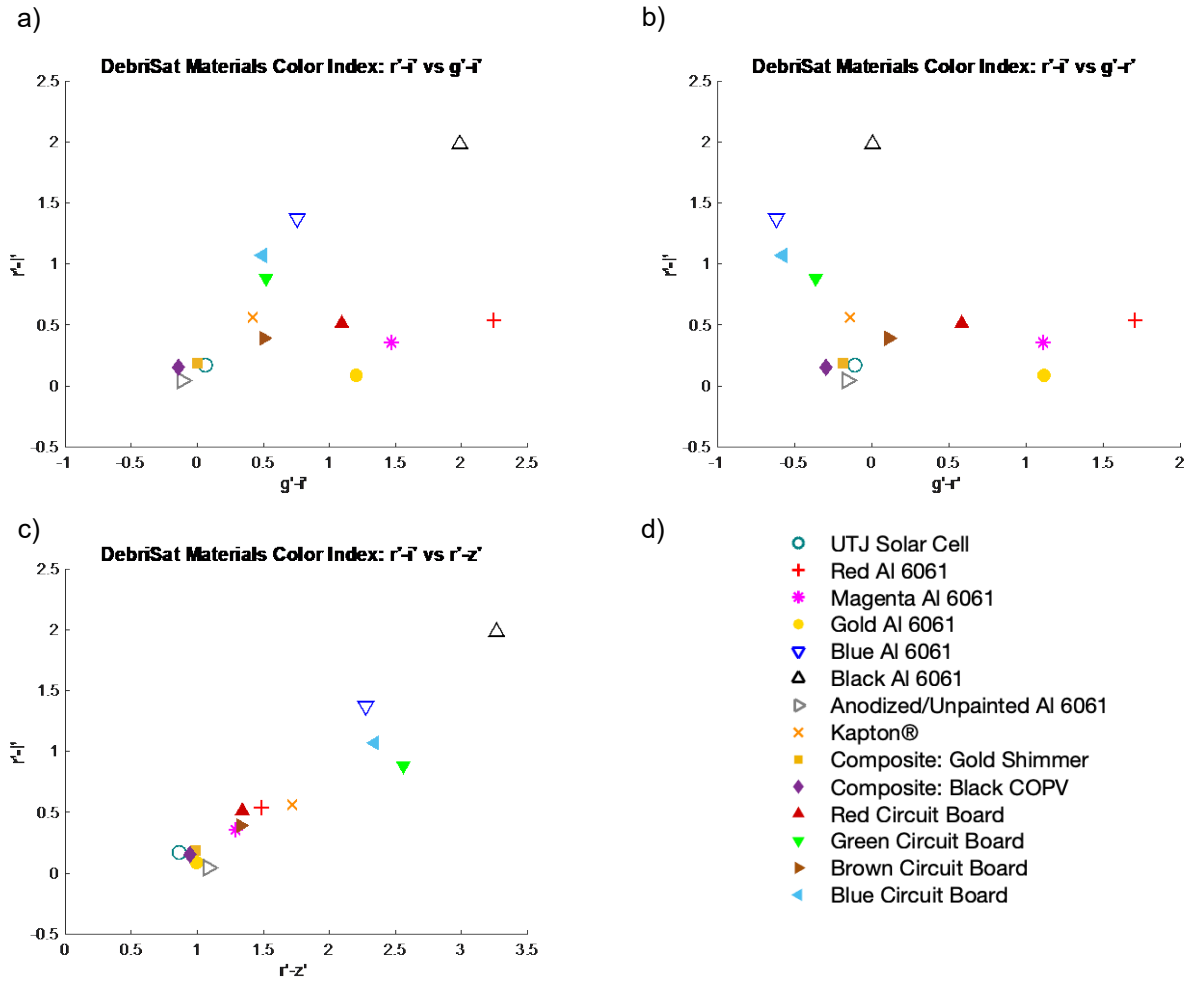

Figure 4. The a) r'- i' versus g'- i' color index plot, b) r'- i' versus g'- r' color index plot, and c) r'- i' versus r'- z' color index plot using SDSS filters for all measured DebriSat material samples in this study. Legend (d) outlines the materials and stars being plotted.

In an attempt to group material samples into families by color value, the color indexes were calculated for each material using different SDSS filters. The color plot comparing r'- i' and g'- i' (Fig. 4a) appears to be most promising when sorting materials by classification. Most of the painted 6061 aluminum alloys have g'- i' values and r'- i' values greater than 0.75 and 0.87 respectively. All circuit board material samples, regardless of color, have their color index values plotted at the center of the r'- i' vs g'- i' plot between 0.039 and 1.07 for r'- i' and 0.49 and 1.09 for g'- i'. The Kapton® polyimide sample has a color index that falls within a section of the r'- i' vs g'- i' plot where the circuit boards are plotted, which can be due to these materials having polymer based compositions. Finding themselves near the lower left corner of the r'- i' vs g'- i' plot are the remaining UTJ solar cell, unpainted anodized 6061 aluminum alloy, and composite samples. The photovoltaic cell and the composites are dark in color, but unlike the black painted alloy, they have a consistently low reflectance response throughout the g', r', and i' filter passbands (Fig. 3). The unpainted anodized alloy is plotted separately from the painted alloys on the r'- i' vs g'- i' plot due to its reflectivity curve resulting in higher values within the g' passband (Fig. 1). This can help better differentiate between unpainted and painted aluminum alloy surfaces.

The r'- i' versus g'- r' (Fig. 4b) and r'- i' versus r'- z' (Fig. 4c) plots did not yield results that were as useful to support the grouping of materials per classification. For these two color index plots, the 6061 painted aluminum alloys resulted in color values that were scattered across the plot and located amongst the circuit board and Kapton® samples, making it difficult to arrange the samples by metal alloy or polymeric categories. Although the solar cell, composites, and unpainted alloy had color index values that remained near each other for all color index plots (Fig. 4a, 4b, 4c), the gold painted 6061 aluminum alloy generated a color value amongst the four aforementioned materials for the r'- i' versus r'- z' plot (Fig. 4c), making this plot unsuitable for assorting material classification by color index values.

From the three color index plots generated in this study using g', r', i', and z' SDSS filters, the r'- i' versus g'- i' plot produced results that were most supportive toward separating materials into their respective categories (metals, polymers, composites, photovoltaics) with each grouping having different material densities. The color values for each material were derived from their reflectivity curves produced from incident light impinging on the material surface. Note that the color index plot data are preliminary results and still need to have solar color value incorporated in each plot to serve as a reference for comparison to the sun.

Reflectance spectra is related to the chemistry for any given material analyzed, producing absorption features in NIR and SWIR that correspond to chemical bonds present within the article's structure. This is why polymers exhibit greater amounts of absorption features in NIR/SWIR than bare metals, why aluminum regularly absorbs light at 850 nm, and why photovoltaics will demonstrate specific features in NIR/SWIR depending on their substrate and stacked structure. There is an evident relationship between reflectance spectra and chemistry. Furthermore, chemistry is related to material density. Hence, it may be possible to directly establish a relationship between reflectance spectra and material density by distinguishing reflectivity and color index trends common between metals, polymers, composites, and photovoltaics. If possible, this information could be used for enhanced prediction of the nature and hazards involved with an object residing in near-Earth orbital regime based on their suggested density.

4. CONCLUSION

Materials commonly incorporated into space hardware have involved aluminum and its alloys, photovoltaics, painted surfaces, multi-layered insulation and polymer-based articles. Composites are emerging as a material on the forefront for current and future space missions. It is essential that remote observations of materials positioned in LEO and GEO are conducted and have the capabilities to identify the nature of those objects. The analysis from these methods can be improved if color index, often used in remote observations, can be related to material density to some degree.

The analysis in this work is a first step toward distinguishing trends between material classifications when provided with their color index values for various telescopic filters. In this study, the Sloan Digital Sky Survey (SDSS) filters were employed for investigation and g', r', i', and z' passbands were used. In the future, color index can be further explored by plotting more combinations of filters against each other. This will help determine which color index plots may best serve as material classification sorters.

Observations in this study involved measurements on DebriSat material samples belonging to different material classifications and were conducted prior to hypervelocity impact. Correlations were drawn in an attempt to group these materials into families according to color index derived from their reflectivity spectral curves. Future work will involve conducting repeatable reflectance measurements on an increased amount of similar space hardware samples to compare the results to conclusions drawn from this study. Color plots using index calculations for each material measured in this study are preliminary results and will need to incorporate solar values in the future to serve as a reference.

5. ACKNOWLEDGEMENTS

The authors would like to thank Dr. Miguel Velez-Reyes from the University of Texas at El Paso for providing multiple resources that contributed to the completion of this research. We would also like to acknowledge NASA Johnson Space Center's Optical Measurements Center (OMC) for providing required capabilities for performing reflectance spectroscopic measurements in optimal conditions. Additionally, we thank the USGS and ECOSTRESS spectral libraries for allowing public access to their data. Jacqueline A. Reyes would like to recognize and thank the NASA Fellowship Activity program (Award #80NSSC18K1702) that is currently supporting her research and academic studies at the University of Texas at El Paso.

6. REFERENCES

[1] M. Matney, A. Manis, P. Anz-Meador, D. Gates, J. Seago, A. Vavrin, and Y.-L. Xu, "The NASA Orbital Debris Engineering Model 3.1: Development, Verification, and Validation," presented at 1st International Orbital Debris Conference, Houston, TX, 2019.

[2] J.-C. Liou, "Collision activities in the future orbital debris environment," *Advances in Space Research*, vol. 38, no. 9, p. 2102-2106, 2006. [Abstract]. Available: ScienceDirect, https://www.sciencedirect.com/science/article/abs/pii/S0273117705008057. [Accessed Feb. 27, 2021].

[3] *Orbital Debris Quarterly News*, NASA Johnson Space Center, Houston, TX, Volume 24, Issue 4, November 2020. [Online], Available: https://orbitaldebris.jsc.nasa.gov/quarterly-news/. [Accessed Feb. 24, 2021].

[4] H.M. Cowardin, J.M. Hostetler, J.I. Murray, J.A. Reyes, and C.L. Cruz, "Optical Characterization of DebriSat Fragments in Support of Orbital Debris Environmental Models," presented at Advanced Maui Optical and Space Surveillance Technologies Conference (AMOS), Maui, HI, 2020.

[5] D. Bedard, M. Levesque, B. Wallace, "Measurement of the photometric and spectral BRDF of small Canadian satellites in a controlled environment," presented at Advanced Maui Optical and Space Surveillance Technologies Conference (AMOS), Maui, HI, 2011.

[6] M. Burke, C. Dawson, C.S. Allen, J. Brum, J. Roberts, and M.P.S. Krekeler, "Reflective spectroscopy investigations of clothing items to support law enforcement, search and rescue, and war crime investigations," *Forensic Science International*, vol. 304, Nov. 2019, 109945.

[7] K. Jorgensen-Abercromby, M. Guyote, and J. Okada, "Inertial Upper Stage Surface Property Study," In Proc. Fourth European Conference on Space Debris, Darmstadt, Germany, 18-20 April 2005.

[8] H.M. Cowardin, "Characterization of Orbital Debris Objects over Optical Wavelengths via Laboratory Measurements," Ph. D. dissertation, University of Houston, Houston, TX, 2010.

[9] J.A. Reyes, B.G. Miller, E.A. Plis, D.C. Ferguson, R.C. Hoffmann, H.M. Cowardin, M.K. Jah, and D.P. Engelhart, "Understanding optical changes in on-orbit spacecraft materials," In Proc. SPIE 11101, Material Technologies and Applications to Optics, Structures, Components, and Sub-Systems IV, 111010E, 30 August 2019, doi: 10.1117/12.2528919.

[10] J. Brum, C. Schlegel, C. Chappell, M. Burke, M.P.S. Krekeler, "Reflective spectra of gasoline, diesel, and jet fuel A on sand substrates under ambient and cold conditions: Implications for detection using hyperspectral remote sensing and development of age estimation models," Environmental Earth Sciences 79, 463, 2020. [Online], Available: https://doi.org/10.1007/s12665-020-09165-2. [Accessed Feb. 26, 2021].

[11] S.K. Meerdink, S.J. Hook, D.A. Roberts, and E.A. Abbott, "The ECOSTRESS spectral library version 1.0," *Remote Sensing of Environment*, vol. 230, Sep. 2019.

[12] R.F. Kokaly, R.N. Clark, G.A. Swayze, K.E. Livo, T.M. Hoefen, N.C. Pearson, R.A. Wise, W.M. Benzel, H.A. Lowers, R.L. Driscoll, and A.J. Klein, USGS Spectral Library Version 7: U.S. Geological Survey Data Series 1035, p. 61, 2017. https://doi.org/10.3133/ds1035.

[13] C. Wang, Q. Chen, M. Hussain, S. Wu, J. Chen, and Z. Tang, "Application of Principal Component Analysis to Classify Textile Fibers Based on UV-Vis Diffuse Reflectance Spectroscopy," *Journal of Applied Spectroscopy*, vol. 84, no. 3, July 2017. DOI 10.1007/s10812-017-0481-8.

[14] S. Hotthaus, T.E.L. Smith, M.J. Wooster, and C.S.B. Grimmond, "Derivation of an urban materials spectral library through emittance and reflectance spectroscopy," ISPRS Journal of Photogrammetry and Remote Sensing, vol. 94, p. 194-212, Aug. 2014. https://doi.org/10.1016/j.isprsjprs.2014.05.005.

[15] H. Cowardin, P. Seitzer, K. Abercromby, E. Barker, and T. Schildknecht, "Characterization of Orbital Debris Photometric Properties Derived from Laboratory-Based Measurements," In Proc. Advanced Maui Optical and Space Surveillance Technologies Conference (AMOS), Maui, HI, 2010.

[16] R.R. Nidamanuri and A.M. Ramiya, "Spectral identification of materials by reflectance spectral library search," *Geocarto International*, vol. 29, no. 6, p. 609-624, 2014.

[17] J.B. Percival, S.A. Bosman, E.G. Potter, et al., "Customized Spectral Libraries for Effective Mineral Exploration: Mining National Mineral Collections," *Clays and Clay Minerals*, vol. 66, no. 3, p. 297-314, 2018.

[18] NASA JSC Spacecraft Materials Spectral Database, NASA Johnson Space Center, Houston, TX, 2021.

[19] I. Marqués, M. Graña, S.M. Sanchez, M.Q. Alkhatib, and M. Velez-Reyes, "Person detection in hyperspectral images via skin segmentation using an active learning approach," In Proc. SPIE 9472, Algorithms and Technologies for Multispectral, Hyperspectral, and Ultraspectral Imagery XXI, 947207, 2015. https://doi.org/10.1117/12.2179333.

[20] M. Werremeyer, "Design of Sub-systems for a Representative Modern LEO Satellite," Dissertation, University of Florida, 2013.

[21] S. Clark, "Design of a Representative LEO Satellite and Hypervelocity Impact Test to Improve the NASA Standard Breakup Model," Dissertation, University of Florida, 2013.

[22] R.R. King, D.C. Law, K.M. Edmondson, C.M. Fetzer, G.S. Kinsey, H. Yoon, R.A. Sherif and N.H. Karam, "40% efficient metamorphic GaInP/GaInAs/Ge multijunction solar cells," *Applied Physics Letter*, vol. 90, no. 18, 2007.

[23] A. Hadj Dida and M. Bekhti, "Study, Modeling and Simulation of the Electrical Characteristic of Space Satellite Solar Cells," presented at 6th International conference on Renewable Energy Research Applications, San Diego, CA, 5-8 Nov. 2017.

[24] A.M. Abd El-Hameed and Y.A. Abdel-Aziz, "Aluminum Alloys in Space Applications: A Short Report", *Journal of Advanced Research in Applied Sciences and Engineering Technology*, vol. 22, no. 1, 2021.

[25] A.M.Abd El-Hameed, Y.A. Abdel-Aziz, and F.S. El-Tokhy, "Anodic Coating Characteristics of Different Aluminum Alloys for Spacecraft Materials Applications," *Materials Sciences and Applications*, vol. 8, p. 197-208, 2017.

[26] *ASM Handbook Volume 2: Properties and Selection: Nonferrous Alloys and Special-Purpose Materials*, vol. 2, ASM International, 1990.

[27] H.E. Boyer and T.L. Gall, *Metals Handbook*, American Society for Metals, Materials Park, OH, 1985.

[28] J.M. Holt, C.Y. Ho, *Structural Alloys Handbook*, CINDAS/Purdue University, West Lafayette, IN, 1996.

[29] D.C. Ferguson, B.V. Vayner, J.T. Galofaro, G. Hillard, J. Vaughn, T. Schneider, "NASA GRC and MSFC Space Plasma Arc Testing Procedures," *IEEE Transactions on Plasma Science*, vol. 34, no. 5, Oct. 2006.

[30] Y.A. Abdel-Aziz, A.M. Abd El-Hameed, F.S. El-Tokhy, A. Ghitas, I. Selim and M. Sabry, "Ground-Based Simulation for the Effects of Space Plasma on Spacecraft," *Advances in Space Research*, vol. 51, no. 1, p. 133-142, 2013. DOI: 10.1016/j.asr.2012.07.026

[31] D. G. Gilmore, *Spacecraft Thermal Control Handbook: Fundamental Technologies*, 2nd ed., The Aerospace Press, El Segundo, 161, 2002.

[32] DuPont™, *DuPont™ Kapton® Summary of Properties*, 2017.

[33] DuPont™, *DuPont™ Kapton® HN Polyimide Film,* 2019.
[34] *'Toray' T1000G Intermediate Modulus Carbon Fiber*, TORAYCA, 2018.
[35] *'Toray' Aerospace Prepreg Selector Guide*, TORAYCA, 2017.
[36] G.R. Devi and K.R. Rao, "Carbon-Carbon Composites – An Overview," *Defence Science Journal*, vol. 43, no. 4, p. 369, 1993.
[37] A. Bulletti, L. Capineri, M. Materassi, and B.D. Dunn, "Surface Resistivity Characterization of New Printed Circuit Board Materials for Use in Spacecraft Electronics," *IEEE Transactions on Electronics Packaging Manufacturing*, vol. 30, no. 2, p. 115-122, 2007.
[38] A.R. Frederickson, E.G. Mullen, K.J. Kerns, P.A. Robinson, and E.G. Holeman, "The CRESS IDM Spacecraft Experiment for Insulator Discharge Pulses," *IEEE Transactions on Nuclear Science*, vol. 40, no. 2, 1993.
[39] "Electro-Isola G-Etronax EP FR4 Epoxy, Glass Fabric Reinforcement, Light Yellow, Sheets," *matweb.com*, MatWeb, LLC., 1996-2021. [Online]. Available: http://www.matweb.com/search/DataSheet.aspx?MatGUID=3c5f252f235844fb9ffec6d1856ba0e3. [Accessed Feb. 28, 2021].
[40] "Rogers Arlon CuClad 217 PTFE/Woven Fiberglass Laminate Microwave Printed Circuit Board Substrate," *matweb.com*, MatWeb, LLC., 1996-2021. [Online]. Available: http://www.matweb.com/search/DataSheet.aspx?MatGUID=952559b637a940658f6ab71767504fdc. [Accessed Feb. 28, 2021].
[41] M. Fukugita, et al., "The Sloan digital sky survey photometric system," *Astronomical Journal*, vol. 111, no. 4, p. 1748-1756, 1996.
[42] F. Campbell, *Elements of metallurgy and engineering alloys*, Materials Park, OH, ASM International, p. 321-322, 2008.
[43] J. Hatch, *Aluminum – Properties and Physical Metallurgy*, Metals Park, OH, American Society of Metals (ASM), ASM International, p. 13-14, 1984.
[44] K. Jorgensen, "Using Reflectance Spectroscopy to Determine Material Type of Orbital Debris," Ph. D. Thesis, University of Colorado, Boulder, CO, 2000.
[45] P.J. Curran, "Remote Sensing of Foliar Chemistry," *Remote Sensing of Environment*, vol. 30, no. 3, p. 271-278, 1989.
[46] J. Mao and F. Bierlein, "Mineral Deposit Research: Meeting the Global Challenge," In Proc. 8th Biennial SGA Meeting, Beijing, China, Aug. 2005.
[47] E.A. Cloutis, "Spectral Reflectance Properties of Hydrocarbons: Remote-Sensing Implications," *Science*, vol. 245, no. 4914, p. 165-168, 1989.